Charge Transport Properties of Multilayer Nanostructures

Daniel M. Schaadt
University of California—San Diego, La Jolla, California, U.S.A.

INTRODUCTION

The demand to increase device speeds and to obtain higher data storage densities leads to decreased device sizes and new device design proposals, of which some were based on multilayer or granular metal/insulator structures, which consist of metallic nanoclusters embedded within an insulating matrix. The design and optimization of devices incorporating these materials require a detailed understanding of the relevant nanoscale electrical transport properties, which can be investigated by scanning probe techniques. This article reviews recent studies of the nanoscale charge transport properties of multilayer or granular metal/insulator structures, and the application of the results of these studies in a novel magnetic field sensor design based on the combination of charge storage and tunnel-magnetoresistance in magnetic discontinuous magnetic multilayer structures is discussed briefly. In particular, charge deposition into Co nanoclusters embedded in a SiO_2 matrix and the decay of the charge as a function of time are discussed. Local charge deposition into and removal from Co nanoclusters was achieved by applying a voltage pulse to a conductive probe tip in a scanning probe microscope. Electrostatic force microscopy (EFM) was used to image charged areas, to determine quantitatively the amount of stored charge, and to characterize charge transport within the Co layer and into the Si substrate. Measurements of decay times for positive and negative charge as a function of nominal Co layer film thickness are presented, and the dynamics of the charge decay for positively and negatively charged nanoclusters is analyzed as a consequence of Coulomb-blockade effects at room temperature considering a detailed model for charge transport within the Co layer as well as from charge Co nanoclusters into the Si substrate.

BACKGROUND

Nanoscale Multilayer Structures

Structures consisting of metallic nanoparticles embedded in an insulating matrix have attracted increasing attention over the past decade because of their new or unusual physical properties and the resulting possible use in various fields and applications such as nonvolatile high density data storage. For instance, the possibility to store electrical charge with long retention times[1,2] in these materials might be used to build nonvolatile floating gate memory devices,[3] or spin-polarized tunneling between ferromagnetic metal nanoparticles embedded in a nonmagnetic insulator[4–8] can be used in magnetic sensors such as read head for hard disks.[9] These materials are generally easy to fabricate by cosputtering of the metal and the oxide and they are very stable both chemically and electrically.[10]

Investigations of nanoscale charge transport properties

The use of granular or discontinuous metal/insulator materials in nonvolatile memory applications or in magnetic field sensors requires a detailed understanding of the charge transport between the metal nanoclusters, which can be measured on a large scale using standard electrodes.[11] However, the reduction of device sizes due to the requirements of increased speed and higher data storage density increases the need to complement large area measurements with investigations of the charge transport properties on the nanoscale, especially in the case of memory applications where charge retention times and decay mechanism are of importance. In recent years, scanning probe microscopes[12] (SPM) have been employed to characterize the properties of locally deposited charge and its decay over time. It was demonstrated that electrical charges can be stored locally in nitride–oxide–semiconductor structures,[13,14] insulator films,[15,16] nanocrystals,[2,17–20] or quantum dots.[21,22] Charge storage in these studies was achieved by applying a bias voltage pulse between the SPM probe tip and the sample. The deposited charge was typically characterized by EFM. Further, studies to investigate charge retention times and decay mechanisms were conducted.[2,23–25] These studies have led to improvements in and better understanding of the measurement techniques,[26,27] have helped to illuminate the charge decay mechanisms in discontinuous Co/SiO_2 multilayer structures,[23] and have resulted in a novel magnetic field sensor design based on the combination of charge storage and tunnel-magnetoresistance in magnetic discontinuous magnetic multilayer structures.[28,29]

Dekker Encyclopedia of Nanoscience and Nanotechnology
DOI: 10.1081/E-ENN 120013808
Copyright © 2004 by Marcel Dekker, Inc. All rights reserved.

Combination of charge storage and tunnel-magnetoresistance in multilayer structures: A new magnetic field sensor

The possibility to store electrical charges with long retention times in a tunnel-magnetoresistive film allows the design of a novel magnetic field sensor design. In this device design, a granular tunnel-magnetoresistive (TMR) $Co_x(SiO_2)_{1-x}$ thin film is placed between two oxide layers within the gate of a p-channel Si metal-oxide-semiconductor-field-effect transistor (MOSFET). Two contacts are placed on the TMR film outside the gate structure. The basic concept is, however, applicable to any field-effect transistor as well as other granular TMR materials, which show the possibility of charge storage in the metal clusters. If fixed voltage V_{MR} is applied across the contacts to TMR film, a current I_{MR} flows through the TMR film and leads to charge Q build-up within the Co nanoclusters. This charge in turn yields a shift in the threshold voltage of the transistor. I_{MR} changes with changing externally applied magnetic field due to spin-dependent tunneling of charge between the Co nanoclusters. Therefore the total charge Q within the gate and thus the transistor threshold voltage V_T are magnetic field dependent. In the prototype device described in Refs. [28] and [29], a maximum threshold voltage shift of approximately 50 mV is reached when the external magnetic field was changed from 0 Oe to the saturation field of about 6 kOe. This results in an absolute change in the transistor saturation current of approximately 30 μA, a factor of 500 larger than the corresponding change in I_{MR}, which is about 60 nA. The absolute change in transistor subthreshold current is about 200 nA, corresponding to a relative change of about 20%. Compared to the relative change in I_{MR} of about 5%, this is an amplification in sensitivity of a factor of four. This demonstrates that the nanoscale charge transport properties of multilayer structures consisting of (magnetic) metal nanoclusters embedded in an insulating matrix can be used in sensor devices with increased performance and are therefore worth investigating in detail.

NANOSCALE CHARGE TRANSPORT EXPERIMENTS

Experimental Procedure

Sample structure and preparation

Samples were prepared by alternating sputtering from two separate targets onto a heavily doped n-type Si (100) substrate covered with a native oxide layer of about ~2.5 nm thickness. The Co was d.c. sputtered and the SiO_2 was rf sputtered. Deposition was performed at room temperature with 2 mTorr Ar pressure. The base pressure in the sputtering system was $\sim 10^{-7}$ Torr. The nominal deposited film structures were SiO_2(3 nm)/Co(1.0–2.0 nm)/SiO_2(3 nm) as determined from the deposition times and rates (0.9–1.3 nm/min for the Co and 2.0–3.0 nm/min for the SiO_2), which were calibrated by low-angle X-ray reflection. Transmission electron microscopy (TEM) studies[7,10,30] have shown that, when deposited on SiO_2, the Co layer is discontinuous with formation of Co nanoclusters, as shown in Fig. 1. The nanoscale structure of the Co layer depends sensitively on the nominal Co film thickness and consists of isolated spherical Co nanoclusters for films with a nominal thickness of approximately less than 1.4 nm and of a chain-like arrangement of spherical Co nanoclusters to tubes of Co for nominal thicker films.[7,10,30]

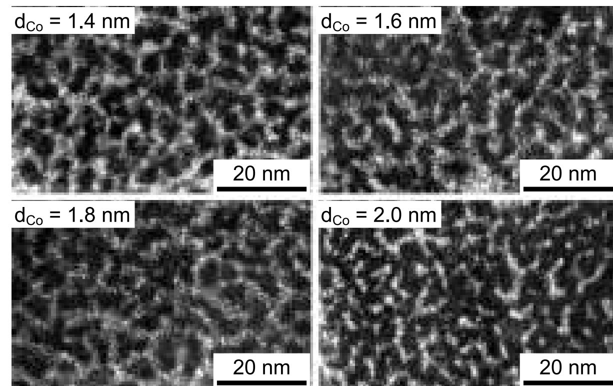

Fig. 1 Plan-view transmission electron micrographs of Co/SiO_2 with varying nominal Co film thickness d_{Co} ranging from 1.4 to 2.0 nm. The light speckled contrast corresponds to amorphous SiO_2 and the dark contrast to crystalline Co. As d_{Co} increases, the Co particles become more connected.

Charge deposition and imaging of deposited charge

Scanning probe studies were performed at room temperature under ambient conditions using a Digital Instruments MultiMode™ Scanning Probe Microscope[a] with a heavily doped p^+-Si tip. Sample charging was achieved during TappingMode™ operation[9] by holding the tip at the center of the scan area for 10 sec with a bias voltage V_{ch} applied to the tip and the sample grounded, as shown in Fig. 2.

[a]MultiMode, TappingMode and LiftMode are trademarks of Digital Instruments, Santa Barbara, CA.

Copyright © Marcel Dekker, Inc. All rights reserved.

Marcel Dekker, Inc.
270 Madison Avenue, New York, New York 10016

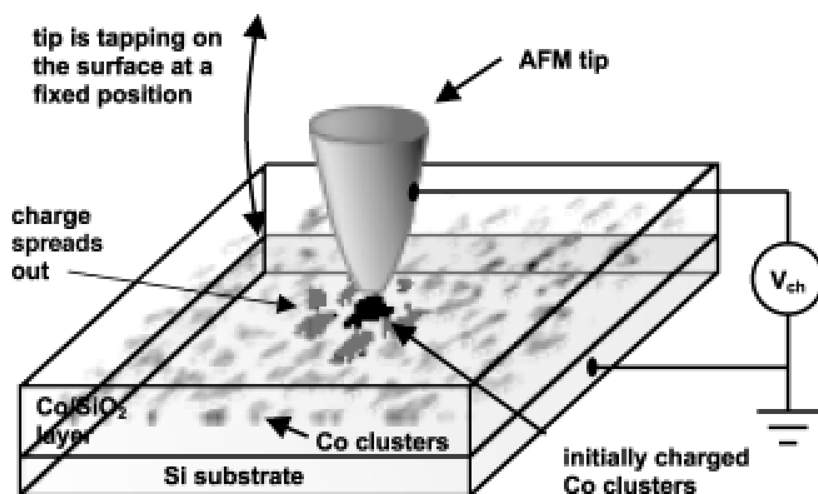

Fig. 2 Schematic diagram showing the charging of Co clusters embedded in the Co/SiO_2 layer. The Si substrate is grounded and a bias voltage V_{ch} is applied to the probe tip, which is tapping on the surface. This causes current to flow from the tip into the Co clusters and from the Co clusters into the Si substrate as well as into neighboring clusters. Charge is initially deposited directly under the tip and spreads out to neighboring clusters.

EFM was used to image charged regions and to estimate the total stored charge. EFM images were obtained using LiftMode.[a] First, a scan line of the topography is recorded using TappingMode. Then the probe tip is lifted about 20 nm above the surface and an imaging bias V_{EFM} is applied. Finally, the probe tip is scanned at the fixed tip-sample distance with VEFM applied by retracing the previously recorded topography scan. During this second scan, the probe tip reacts to long-range forces such as electrostatic interactions between the deposited charge in the sample and its image charge in the probe tip.

The contrast observed in the EFM image may be used to calculate the total stored charge Q. An exact calculation of the deposited charge can be complicated because of the complex arrangement of image charges in the probe tip and the sample.[27] Possible artifacts in the topography scan due to electrostatic forces between the image and these charges can lead to an incorrectly measured topography and can cause difficulties separating EFM contrast from topography. However, if the deposited charge is small, its influence on the topography scan is minimal and might not lead to these artifacts. Further, if the tip-sample separation is large enough and the deposited charge small, the EFM response becomes symmetric with respect to imaging bias V_{EFM}.[27] It is easy to check if these conditions are met by imaging the topography after charge has been deposited and by recording the EFM signal for opposite imaging voltages. Assuming that no artifacts are visible before and after charging in the topography and the EFM signal is symmetric with respect to V_{EFM}, a simple approach can be used to estimate the deposited charge. Specifically, the shift Δf in the resonant frequency of the cantilever is related to the force gradient $F' \equiv dF/dz$ by the expression.[31]

$$\Delta f = -f_0 F'(z_0)/(2k) \tag{1}$$

where $z_0 = 20$ nm is the lift height during EFM imaging, $f_0 = 232$ kHz the cantilever resonant frequency, and k the cantilever spring constant, which was calculated from the lever geometry to be 90 ± 10 N/m. The force $F(z)$ arises from Coulomb interactions of the stored charge, its image charges in the tip and Si substrate, and the induced charges due to the voltage V_{EFM} applied during imaging. From an electrostatic analysis of the tip-sample system modeled using a simple parallel-plate geometry, the force is found to be given by[2]

$$F(z) = \frac{1}{(z + (d_1 + d_2)/\varepsilon_{SiO_2})^2} \times \left(-\frac{d_2^2 Q^2}{\varepsilon_{SiO_2}^2 \varepsilon_0 A} + \frac{2 d_2 Q V_{EFM}}{\varepsilon_{SiO_2}} + \frac{\varepsilon_0 A V_{EFM}^2}{2} \right) \tag{2}$$

where d_1 and d_2 are the thicknesses of the top and bottom oxide layer, respectively, ε_{SiO_2} the relative dielectric constant of SiO_2, z the tip-sample separation, and A the area of the charged region. If the deposited charge Q is small, the first term in the bracket in Eq. 2 is small. The third term in the bracket is independent of the stored charge and yields a constant background frequency shift at all points in the EFM image. Thus the final contrast

Copyright © Marcel Dekker, Inc. All rights reserved.

observed is proportional to the stored charge Q and to V_{EFM}. Using the values for f_0, k, z, d_1, and d_2 given above, the total charge Q is then given by

$$Q = 18 \pm 2e/\mathrm{V} \cdot \mathrm{Hz}\ V_{EFM}\Delta f \quad (3)$$

As mentioned above and provided that Q is small, the EFM response Δf is symmetric with respect to V_{EFM}, which can be readily checked in control experiments.

Results and Discussion

Nanoscale charge storage

A series of topography and EFM images obtained with $V_{EFM} = 1$ V and $V_{EFM} = -1$ V before and after charging of a nominally 1.4-nm-thick Co layer with $V_{ch} = -12$ V for 10 sec are shown in Fig. 3. No image-charge artifacts are observed in the topography and EFM images before charging. After charging, charged areas are observed in the EFM images as peaks or dips with a symmetric resonant frequency shift of about 1 and -1 Hz, depending on the relative sign of the imaging voltages. No charge-induced artifacts are observed in the topography images after charge has been deposited, and measurements with $V_{EFM} = 0$ V are showing no contrast difference between charged and uncharged regions. Such a contrast difference would be expected if the amount of deposited charge is large enough to cause an attractive force between the deposited charge and its image charge in the tip.[27] The above observations suggest, however, that the amount of deposited charge Q is small and therefore the simplified approach to estimate Q from the EFM contrast, as described above, can be used.

No charging was observed in a control sample in which no Co layer was present, and it is therefore concluded that the deposited charge is stored in the Co layer. Little variation in sample charging was observed for charging times longer than 5 sec. Deposited charge can be erased by applying a voltage pulse of opposite sign.[23]

The charging of the Co/SiO_2 film is believed to occur in the following way: when the tip approaches the sample surface, charges tunnel from the tip through the top oxide layer into the Co clusters. At the same time, charges tunnel to neighboring uncharged Co clusters and through the thicker bottom oxide layer into the Si substrate. The currents that charge and decharge clusters are initially different because of the different oxide thicknesses of the top oxide layer and the oxide layer between the Co clusters and the Si substrate. These currents equilibrate over time as a consequence of the adjustments in the electric fields across the oxide layers due to the charge build-up in the Co layer, in a manner analogous to the charging process in a floating-gate MOS structure. Once equilibrium is reached, the charge in the Co layer does not increase any further and its value is determined by the tip-sample capacitance.

Nanoscale charge transport

Previous measurements have shown that the deposited charge decays over time, with most of the stored charge tunneling into the Si substrate and some carrier transport also occurring between Co nanoclusters.[23] Decay times for positive and negative charges were measured and a strong dependence on the nanoscale Co film structure was observed. However, because of the difficulties in extracting the exact amount of charge as a function of

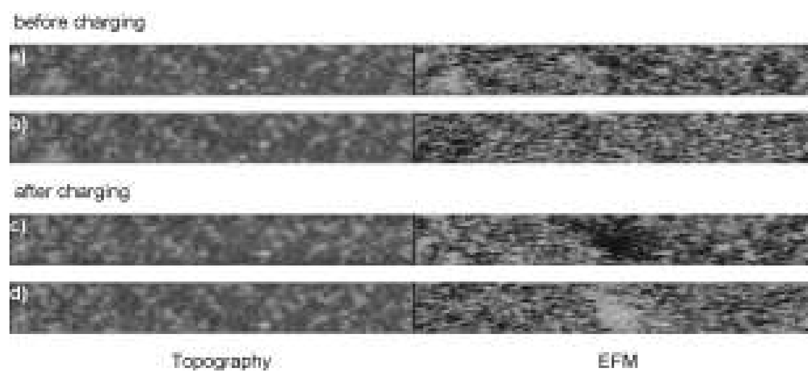

Fig. 3 Topography (left) and EFM images (right) before charging using (a) $V_{EFM} = 1$ V and (b) $V_{EFM} = -1$ V, and after charging using (c) $V_{EFM} = 1$ V and (d) $V_{EFM} = -1$ V. Charge was deposited with $V_{ch} = -12$ V for 10 sec. The image sizes are 500 nm by 2 μm. There are no image-charge-induced artifacts visible in the topography and EFM images before charging. After charging, the topography images show no artifacts due to the deposited charge, while the EFM images show a peak and dip with a height of about 1 and -1 Hz, respectively.

Copyright © Marcel Dekker, Inc. All rights reserved.

time after charging, large error bars were observed in the decay times. To overcome the uncertainties and to confirm these measurements, additional measurements and analysis were performed. Fig. 4 shows the decay in charge for regions charged at 12 V and −12 V for various nominal Co layer film thicknesses. The charge decay appears exponential in all cases, but with different decay times τ_+ and τ_- for positive and negative stored charge, respectively.

The difference in the decay times for positive and negative charging can be interpreted as a consequence of the Coulomb blockade energy $E_0 = q^2/(2C_{Co})$ of a single Co cluster with capacitance C_{Co}. Assuming in a first approximation that charge decay occurs only between Co clusters and the Si substrate, this leads to a difference in barrier heights for escape of positive and negative charge, given, respectively, by $\phi_+ = \phi_0 + E_0$ and $\phi_- = \phi_0 - E_0$, where $\phi_0 = (\phi_{Co} + \chi_{Si} - 2\chi_{SiO_2})/2$ is the barrier height of the Co–SiO_2–Si tunnel barrier, ϕ_{Co} the Co workfunction, χ_{Si} the Si electron affinity, χ_{SiO_2} the SiO_2 electron affinity, and q the electron charge. As the dependence of the tunneling probability T on barrier height ϕ and barrier thickness d is given approximately by $T \propto \exp(-2d\sqrt{2mq\phi}/\hbar)$ and the retention is inversely

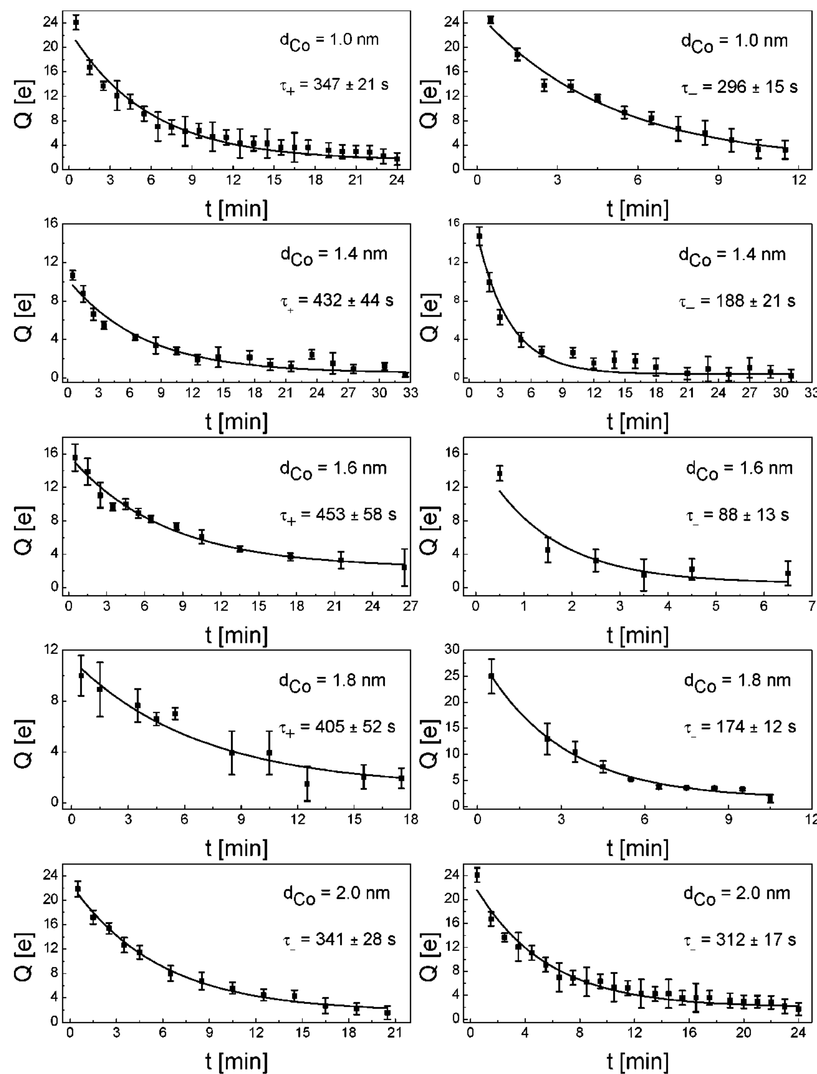

Fig. 4 Decay of positive charge (left column) and negative charge (right column) for Co/SiO_2 films with nominal Co film thickness ranging from 1.0 to 2.0 nm. The retention times τ_+ and τ_-, obtained by first-order exponential fits to the peak height for positive charge and the valley depth for negative charge in the EFM images, respectively, depend strongly on the nominal Co film thickness. The retention time τ_+ for positive charge is for all film thicknesses larger than the retention time τ_- for negative charge.

Copyright © Marcel Dekker, Inc. All rights reserved.

Marcel Dekker, Inc.
270 Madison Avenue, New York, New York 10016

ORDER REPRINTS

proportional to T,[2] the relation between the decay times is given approximately by

$$\frac{\tau_+}{\tau_-} \approx e^{\frac{2\sqrt{2m}}{\hbar} d_{SiO_2}\left(\sqrt{q\phi_0+E_0}-\sqrt{q\phi_0-E_0}\right)}$$

$$\approx 1 + \frac{2\sqrt{2m}}{\hbar}\frac{d_{SiO_2}}{\sqrt{q\phi_0}}E_0 \text{ for } E_0 \ll q\phi_0 \tag{4}$$

Solving Eq. 4 for the charging energy and using the measured values for τ_+ and τ_- of the nominally 1.4-nm-thick Co layer, we obtain E_0 = 33±6 meV. As seen in the TEM image shown in Fig. 1, the Co particles are roughly spherical with a radius of ~1.5 nm and are roughly arranged in chains with typical lengths of 3–6 particles for a nominally 1.4-nm-thick Co film. The charging energy of such nanoclusters is approximately 31±10 meV, which is in very good agreement with the value estimated from measured decay times. The Coulomb-blockade energy E_0 depends strongly on the size and shape of the Co cluster, and it is observed that the retention times depend strongly on the nanoscale structure of the Co layer. Fig. 5 shows the retention times τ_+ for positive charge and τ_- for negative charge as functions of the nominal Co film thickness. The results are comparable to the previously measured retention times but show smaller errors in the values. τ_+ first increases with increasing d_{Co}, reaching a maximum for

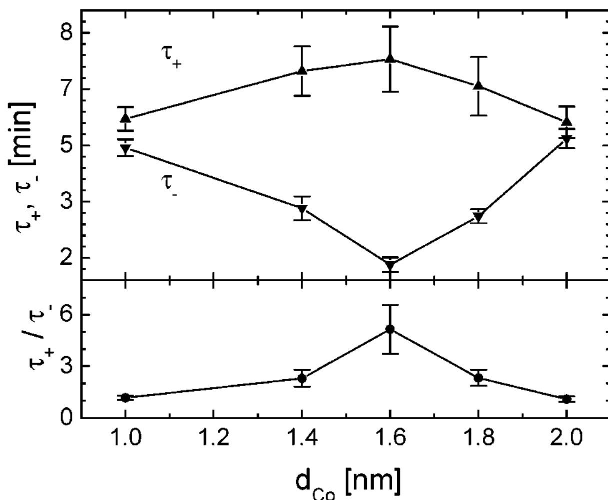

Fig. 5 Retention times for τ_+ positive charge and τ_- for negative charge and the ratio τ_+/τ_- plotted as functions of nominal Co film thickness d_{Co}. τ_+ first increases with increasing d_{Co}, reaching a maximum for d_{Co}=1.6 nm, and then decreases and approaches τ_-. In contrast, the negative charge retention time τ_- shows the opposite behavior, first decreasing with increasing d_{Co}, reaching a minimum for d_{Co}=1.6 nm, and then increasing with increasing d_{Co}.

d_{Co}=1.6 nm, and then decreases and approaches τ_-. In contrast, the negative charge retention time τ_- shows the opposite behavior, first decreasing with increasing d_{Co}, reaching a minimum for d_{Co}=1.6 nm, and then increasing with increasing d_{Co}. As expected from the above simplified model, the retention time for positive charge is larger than that for negative charge over the entire range of values of d_{Co}, and for d_{Co} larger than 1.6 nm the difference in retention times becomes smaller as d_{Co} increases, i.e., as the Coulomb blockade energy decreases. However, the decreasing difference in retention times with decreasing d_{Co} below 1.4 nm is not expected from the simplified model. This behavior of the retention times can be explained by a model including discharging from the Co nanoclusters into the Si substrate and charge decay within the Co layer. The total retention times τ_+ and τ_- will then be given by

$$\frac{1}{\tau_{+,-}} = \frac{1}{\tau^{in}_{+,-}} + \frac{1}{\tau^{out}_{+,-}} \tag{5}$$

where τ^{in}_+ and τ^{in}_- are the characteristic retention times for charge transport within the Co layer and τ^{out}_+ and τ^{out}_- pertain to charge transport from the Co layer into the Si substrate. As the retention times depend strongly on the barrier width as well as the Coulomb-blockade energy, it is necessary to account for the nanoscale structure of the Co layer. It is known from TEM micrographs that the Co layer consists of isolated spherical clusters for a nominal layer thickness of about 1.4 nm and below, and of chainlike or tubelike arrangements of connected spherical particles for nominally thicker films.[7,10,30] As the Co clusters increase in size with increasing nominal thickness above 1.4 nm, the capacitance of these clusters increases and thus the Coulomb-blockade energy decreases. As the nominal film thickness decreases below about 1.4 nm, the Co particles remain spherical and the spacing between the particles increases.[7,10,30] Thus the Coulomb-blockade energy remains fairly constant below nominal thicknesses of about 1.4 nm.

For discharging within the Co layer, the retention times are given by[23]

$$\tau^{in}_{+,-} \propto e^{\frac{2\sqrt{2m^{h,e}_{SiO_2}}}{\hbar} d_{sp}\sqrt{q\phi_{Co}-q\chi_{SiO_2}\pm E_0}} \tag{6}$$

where d_{sp} is the spacing between the Co clusters, and $m^h_{SiO_2}$ and $m^e_{SiO_2}$ are the effective mass of holes and electrons in SiO_2, respectively. τ^{in}_+ and τ^{in}_- increase exponentially with increasing d_{sp} as the nominal Co film thickness decreases below 1.4 nm, and approach each other as E_0 decreases for Co films with nominal thickness above 1.4 nm. For small Coulomb-blockade energies $E_0 \leq kT$, where k is the Boltzmann constant, a

Copyright © Marcel Dekker, Inc. All rights reserved.

Marcel Dekker, Inc.
270 Madison Avenue, New York, New York 10016

hole will tunnel from the Co cluster into the conduction band of the Si substrate, and τ_+^{out} is given by[23]

$$\begin{aligned}\tau_+^{out} &\propto e^{\frac{2\sqrt{2q}}{\hbar}\int_0^{d_{SiO_2}+W}\sqrt{m^h\phi(x)}dx} \\ &\approx e^{\frac{2\sqrt{2}}{\hbar}\left(d_{SiO_2}\sqrt{m^h_{SiO_2}(q\phi_0+E_0)}+\frac{\pi}{2}W\sqrt{qm^h_{Si}V_{bi}}\left(1+\frac{E_0}{qV_{bi}}\right)-W\sqrt{2m^h_{Si}E_0}\right)}\end{aligned} \quad (7)$$

where the barrier height is given by $\phi(x) = \phi_{Co} - \chi_{SiO_2} + E_0/q + (\chi_{Si} - \phi_{Co})x/d_{SiO_2}$ for $0 \le x \le d_{SiO_2}$ and $\phi(x) = V_{bi} + E_0/q - V_{bi}(x - d_{SiO_2})^2/W^2$ for $d_{SiO_2} < x < d_{SiO_2} + W$, m^h_{Si} is the effective hole mass in Si, $W = \sqrt{2\varepsilon_{Si}V_{bi}/(qN_C)}$ is the depletion width, ε_{Si} is the Si permittivity, N_C the effective density of states in the Si conduction band, and V_{bi} the built-in potential. As the Coulomb-blockade energy increases with decreasing d_{Co}, τ_+^{out} increases.

For Coulomb-energies in the range $kT < E_0 < E_g - qV_{bi} - kT$, where E_g is the Si bandgap, no hole states exist on the semiconductor side. The tunneling probability becomes very small and thus the retention time τ_+^{out} reaches a maximum value. According to Eq. 5, the total retention time τ_+ for positive charge will be limited by τ_+^{in} in this regime.

Finally, for Coulomb energies $E_0 \ge E_g - qV_{bi} - kT$, tunneling of holes into the valence band is possible, and τ_+^{out} is given by[23]

$$\tau_+^{out} \propto e^{\frac{2\sqrt{2m^h_{SiO_2}}}{\hbar}d_{SiO_2}\sqrt{q\phi_0+E_0+(E_g-qV_{bi})/2}} \quad (8)$$

For tunneling from a negatively charged Co cluster into the Si substrate, the tunneling barrier width depends on the Coulomb-blockade energy E_0 due to the band bending within the Si substrate layer. τ_-^{out} is then given, in a manner analogous to that used to obtain Eq. 7, by[23]

$$\tau_-^{out} \propto e^{\frac{2\sqrt{2}}{\hbar}\left(d_{SiO_2}\sqrt{m^e_{SiO_2}(q\phi_0-E_0)}+\frac{\pi}{2}W\sqrt{qm^e_{Si}V_{bi}}\left(1-\frac{E_0}{qV_{bi}}\right)\right)} \quad (9)$$

where m^e_{Si} is the effective electron mass in Si.

The expressions for $\tau_{+,-}^{in}$, $\tau_{+,-}^{out}$, and $\tau_{+,-}$ derived in Eqs. 5–9 may be used to analyze the dependence of $\tau_{+,-}$ on d_{Co}. As exact values for the Coulomb-blockade energies and the spacing between Co clusters are unknown or difficult to extract from TEM images, the following values are assumed, which are believed to be physically reasonable. A value of 2.05 nm was assumed for d_{sp} for d_{Co} = 1.0 nm, decreasing linearly to 2 nm for d_{Co} = 1.4 nm and then remaining constant for d_{Co} > 1.4 nm. E_0 is assumed to decrease linearly from 0.11 to 0.01 eV for d_{Co} increasing from 1.0 to 2.0 nm. The computed dependence of τ_+ and τ_- on d_{Co}, as shown in Fig. 6, qualitatively reproduces the experimentally

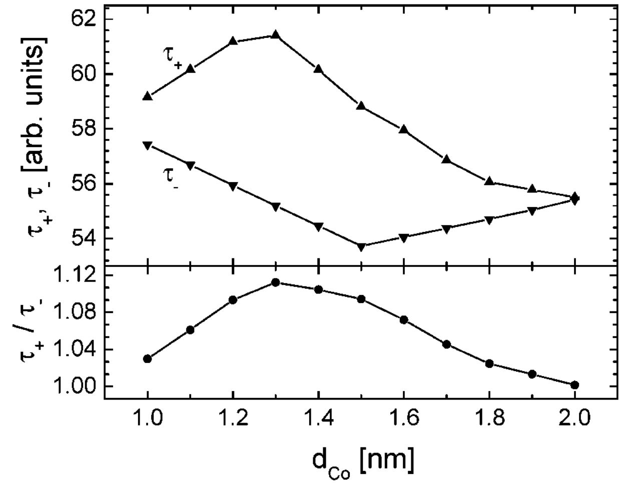

Fig. 6 Calculated retention times as functions of nominal Co film thickness. The computed curves follow the measured curves qualitatively but cannot reproduce the exact behavior because of uncertainties in the Coulomb blockade energies of the Co clusters and the detail band structure.

observed dependence quite closely. However, discrepancies exist between the measured and simulated values because of the uncertainties in the estimation of values such as the Coulomb energies, barrier thicknesses, and barrier heights.

CONCLUSION

The use of granular or discontinuous metal/insulator materials in memory or sensor devices requires a detailed understanding of the nanoscale charge transport, which can be investigated by scanning probe techniques. Electrostatic force microscopy was used to demonstrate and characterize local charge deposition and transport in Co nanoclusters embedded in an insulating SiO_2 matrix. Positive and negative charge can be deposited controllably and reproducibly in such nanoclusters, typically in quantities of ~5–20 electrons within areas 30–50 nm in radius. The charge decays over several minutes with part of it spreading out in the discontinuous Co film and the rest tunneling into to Si substrate. The charge retention times τ_+ for positive charge and τ_- for negative charge as well as their ratio depend strongly on the nanoscale structure of the discontinuous metal cluster film. These results were interpreted as a consequence of Coulomb-blockade effects, and a detailed model considering charge transport within the Co layer as well as from the Co cluster into the Si substrate was used to explain the dependence of the retention times on the nanoscale Co/SiO_2 film

Copyright © Marcel Dekker, Inc. All rights reserved.

ORDER REPRINTS

structure qualitatively. These studies have led to a novel magnetic field sensor design based on the combination of charge storage and tunnel-magnetoresistance of the Co/SiO_2 film, which shows a significant improvement in magnetic field sensitivity as compared to the tunnel-magnetoresistance of the Co/SiO_2 film alone. Incorporation of a granular metal/insulator magnetoresistive film into the gate of a field-effect transistor structure allows the magnetoresistive response to be converted to a shift in the threshold voltage of the transistor, resulting in a large amplification in sensitivity to an external magnetic field. In a prototype device based on a p-channel MOSFET, a threshold voltage shift of 50 mV upon application of a 6-kOe magnetic field was obtained at room temperature. This resulted in a fourfold amplification in relative current response, and an increase in absolute current response by a factor of 500 in the saturation regime, as compared to the response attainable in the magnetoresistive film alone.

ACKNOWLEDGMENTS

Part of this work was supported by NSF (Award No. ECS95-01469 and DMR 9400439) and ONR (Grant No. N00014-95-1-0996). I thank S. Sankar and A.E. Berkowitz for the preparation of the Co/SiO_2 films and for providing me with TEM micrographs of these films. Special thank goes to E.T. Yu for support, guidance, and helpful discussions. I also acknowledge helpful comments from P.M. Asbeck and S.S. Lau.

REFERENCES

1. Boer, E.A.; Brongersma, M.L.; Atwater, H.A.; Flagan, R.C.; Bell, L.D. Localized charge injection in SiO_2 films containing silicon nanocrystals. Appl. Phys. Lett. **2001**, *79* (6), 791–793.
2. Schaadt, D.M.; Yu, E.T.; Sankar, S.; Berkowitz, A.E. Charge storage in Co nanoclusters embedded in SiO_2 by scanning force microscopy. Appl. Phys. Lett. **1999**, *74* (3), 472–474.
3. Tiwari, S.; Rana, F.; Hanafi, H.; Hartstein, A.; Crabbé, E.F.; Chan, K. A silicon nanocrystals based memory. Appl. Phys. Lett. **1996**, *68* (10), 1377–1379.
4. Gittleman, J.I.; Goldstein, Y.; Bozowski, S. Magnetic properties of granular nickel films. Phys. Rev., B **1972**, *5* (9), 3609–3621.
5. Coffey, K.R.; Hylton, T.L.; Parker, M.A.; Howard, J.K. Thin film structures for low field granular giant magnetoresistance. Scr. Metall. Mater. **1995**, *33* (10–11), 1593–1602.
6. Sankar, S.; Dieny, B.; Berkowitz, A.E. Spin-polarized tunneling in discontinuous CoFe/HfO_2 multilayers. J. Appl. Phys. **1997**, *81* (8), 5512–5514.
7. Sankar, S.; Berkowitz, A.E.; Smith, D.J. Spin-dependent tunneling in discontinuous Co–SiO_2 magnetic tunnel junctions. Appl. Phys. Lett. **1998**, *73* (4), 535–537.
8. Dinia, A.; Schmerber, G.; Ulhaq, C.; El Bahraoui, T. Magnetic and transport properties of discontinuous metal-oxides multilayers. Mater. Sci. Eng. **2003**, *B97*, 231–234.
9. Parker, M.A.; Coffey, K.R.; Howard, J.K.; Tsang, C.H.; Fontana, R.E.; Hylton, T.L. Overview of progress in giant magnetoresistive sensors based on NiFe/Ag multilayers. IEEE Trans. Magn. **1996**, *32* (1), 142–148.
10. Dieny, B.; Sankar, S.; McCartney, M.R.; Smith, D.J.; Bayle-Guillemaud, P.; Berkowitz, A.E. J. Magn. Magn. Mater. **1998**, *185* (3), 283–292.
11. Kakazei, G.N.; Lopes, A.M.L.; Pogorelov, Y.G.; Santos, J.A.M.; Sousa, J.B.; Freitas, P.P.; Cardoso, S.; Snoeck, E. Time-dependent transport effects in CoFe/Al_2O_3 discontinuous multilayers. J. Appl. Phys. **2000**, *87* (9), 6328–6330.
12. Binnig, G.; Quate, C.F.; Gerber, C. Atomic force microscope. Phys. Rev. Lett. **1986**, *56* (9), 930–933.
13. Barrett, R.C.; Quate, C.F. Charge storage in a nitride–oxide–silicon medium by scanning capacitance microscopy. J. Appl. Phys. **1991**, *70* (5), 2725–2733.
14. Dreyer, M.; Wiesendanger, R. Scanning capacitance microscopy and spectroscopy applied to local charge modifications and characterization of nitride–oxide–silicon heterostructures. Appl. Phys. **1995**, *A61* (4), 357–362.
15. Terris, B.D.; Stern, J.E.; Rugar, D.; Mamin, H.J. Contact electrification using force microscopy. Phys. Rev. Lett. **1989**, *63* (24), 2669–2772.
16. Terris, B.D.; Stern, J.E.; Rugar, D.; Mamin, H.J. Localized charge force microscopy. J. Vac. Sci. Technol., A **1990**, *8* (1), 374–377.
17. Jones, J.T.; Bridger, P.M.; Marsh, O.J.; McGill, T.C. Charge storage in CeO_2/Si/CeO_2/Si(111) structures by electrostatic force microscopy. Appl. Phys. Lett. **1999**, *75* (9), 1326–1328.
18. Boer, E.A.; Bell, L.D.; Brongersma, M.L.; Atwater, H.A.; Ostraat, M.L.; Flagan, R.C. Charging of single Si nanocrystals by atomic force microscopy. Appl. Phys. Lett. **2001**, *78* (20), 3133–3135.
19. Mélin, T.; Deresmes, D.; Stiévenard, D. Charge

Copyright © Marcel Dekker, Inc. All rights reserved.

injection in individual silicon nanoparticles deposited on a conductive substrate. Appl. Phys. Lett. **2002**, *81* (26), 5054–5056.
20. Decossas, S.; Mazen, F.; Baron, T.; Souifi, A.; Brémond, G. Electric measurements by AFM on silicon nanocrystals. Physica E **2003**, *17*, 543–545.
21. Tevaarwerk, E.; Rugheimer, P.; Castellini, O.M.; Keppel, D.G.; Utley, S.T.; Savage, D.E.; Lagally, M.G.; Eriksson, M.A. Electrically isolated SiGe quantum dots. Appl. Phys. Lett. **2002**, *80* (24), 4626–4628.
22. Guillemot, C.; Budau, P.; Chevrier, J.; Marchi, F.; Comin, F.; Alandi, C.; Bertin, F.; Buffet, N.; Wyon, Ch.; Mur, P. Imaging of stored charges in Si quantum dots by tapping and electrostatic force microscopy. Eur. Phys. Lett. **2002**, *59* (4), 566–571.
23. Schaadt, D.M.; Yu, E.T.; Sankar, S.; Berkowitz, A.E. Proximal probe characterization of nanoscale charge transport properties in Co/SiO_2 multilayer structures. J. Electron. Mater. **2000**, *29* (11), 1299–1303.
24. Felidj, N.; Lambert, J.; Guthmann, C.; Saint-Jean, M. Charge stability on thin insulators studied by atomic force microscopy. Eur. Phys. J. AP **2000**, *12*, 85–91.
25. Buh, G.H.; Chung, H.J.; Kuk, Y. Real-time evolution of trapped charge in a SiO_2 layer: An electrostatic force microscopy study. Appl. Phys. Lett. **2001**, *79* (13), 2010–2012.
26. Boer, E.A.; Bell, L.D.; Brongersma, M.L.; Atwater, H.A. Models for quantitative charge imaging by atomic force microscopy. J. Appl. Phys. **2001**, *90* (6), 2764–2772.
27. Lambert, J.; Guthmann, C.; Saint-Jean, M. Relationship between charge distribution and its image by electrostatic force microscopy. J. Appl. Phys. **2003**, *93* (9), 5369–5376.
28. Schaadt, D.M.; Yu, E.T.; Sankar, S.; Berkowitz, A.E. A monolithic field-effect-transistor-amplified magnetic field sensor. Appl. Phys. Lett. **1999**, *75* (5), 731–733.
29. Schaadt, D.M.; Yu, E.T.; Sankar, S.; Berkowitz, A.E. Characterization and analysis of a novel hybrid magnetoelectronic device for magnetic field sensing. J. Vac. Sci. Technol., A **2000**, *18* (4), 1834–1837.
30. Sankar, S. *Correlation of Microstructural, Magnetic, and Transport Properties of Composite Metal-Insulator Films, UMI Microform 9963657*; Bell & Howell Information and Learning Company: Ann Arbor, MI, 2000; 50.
31. Martin, Y.; Williams, C.C.; Wickramasinghe, H.K. Atomic force microscope-force mapping and profiling on a sub 100-AA scale. J. Appl. Phys. **1987**, *61* (10), 4723–4729.

Copyright © Marcel Dekker, Inc. All rights reserved.

Marcel Dekker, Inc.
270 Madison Avenue, New York, New York 10016